AD-A054 618 AEROSPACE CORP EL SEGUNDO CALIF IVAN A GETTING LABS F/G 3/2
CORONAL MAGNETIC - FIELD MODEL WITH NONSPHERICAL SOURCE SURFACE--ETC(U)
APR 78 M SCHULZ, E N FRAZIER, D J BOUCHER F04701-77-C-0078
UNCLASSIFIED TR-0078(3960-06)-2 SAMSO-TR-78-86 NL

| OF |
AD
A054618

END
DATE
FILMED
6-78
DDC

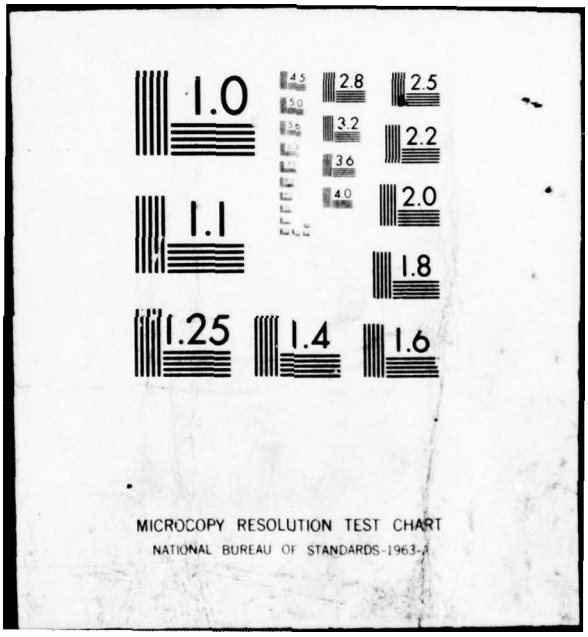
1.0
1.1
1.25
1.4
1.6
1.8
2.0
2.2
2.5
2.8
3.2
3.6
4.0
4.5
5.0
5.6
MICROCOPY RESOLUTION TEST CHART
NATIONAL BUREAU OF STANDARDS-1963-A

REPORT SAMSO-TR- 78-86

Coronal Magnetic-Field Model With Nonspherical Source Surface

Prepared by M. SCHULZ, E. N. FRAZIER, and D. J. BOUCHER, Jr.
Space Sciences Laboratory
The Ivan A. Getting Laboratories
The Aerospace Corporation
El Segundo, Calif. 90245

25 April 1978

Interim Report

Prepared for

SPACE AND MISSILE SYSTEMS ORGANIZATION
AIR FORCE SYSTEMS COMMAND
Los Angeles Air Force Station
P.O. Box 92960, Worldway Postal Center
Los Angeles, Calif. 90009

This interim report was submitted by The Aerospace Corporation, El Segundo, CA 90245, under Contract No. F04701-77-C-0078 with the Space and Missile Systems Organization, Deputy for Advanced Space Programs, P.O. Box 92960, Worldway Postal Center, Los Angeles, CA 90009. It was reviewed and approved for The Aerospace Corporation by G. A. Paulikas, Director, Space Sciences Laboratory. Lieutenant Dara Batki, SAMSO/YCPT, was the project officer for Advanced Space Programs.

This report has been reviewed by the Information Office (OI) and is releasable to the National Technical Information Service (NTIS). At NTIS, it will be available to the general public, including foreign nations.

This technical report has been reviewed and is approved for publication. Publication of this report does not constitute Air Force approval of the report's findings or conclusions. It is published only for the exchange and stimulation of ideas.

Dara Batki

Dara Batki, Lt, USAF
Project Officer

Robert W. Lindemuth

Robert W. Lindemuth, Lt Col, USAF
Chief, Technology Plans Division

Floyd R Stuart

FLOYD R. STUART, Colonel, USAF
Deputy for Advanced Space Programs

FOR THE COMMANDER

UNCLASSIFIED

SECURITY CLASSIFICATION OF THIS PAGE (When Data Entered)

REPORT DOCUMENTATION PAGE	READ INSTRUCTIONS BEFORE COMPLETING FORM
1. REPORT NUMBER: SAMSO-TR-78-86	2. GOVT ACCESSION NO.
3. RECIPIENT'S CATALOG NUMBER	
4. TITLE (and Subtitle): CORONAL MAGNETIC-FIELD MODEL WITH NONSPHERICAL SOURCE SURFACE.	5. TYPE OF REPORT & PERIOD COVERED: Interim rept.
	6. PERFORMING ORG. REPORT NUMBER: TR-0078(3960-06)-2
7. AUTHOR(s): Michael Schulz, Edward N. Frazier and Donald J. Boucher, Jr.	8. CONTRACT OR GRANT NUMBER(s): F04701-77-C-0078
9. PERFORMING ORGANIZATION NAME AND ADDRESS: The Aerospace Corporation, El Segundo, Calif. 90245	10. PROGRAM ELEMENT, PROJECT, TASK AREA & WORK UNIT NUMBERS
11. CONTROLLING OFFICE NAME AND ADDRESS: Space and Missile Systems Organization, Air Force Systems Command, Los Angeles, Calif. 90009	12. REPORT DATE: 25 April 1978
	13. NUMBER OF PAGES: 51
14. MONITORING AGENCY NAME & ADDRESS (if different from Controlling Office) 53 pp.	15. SECURITY CLASS. (of this report): Unclassified
	15a. DECLASSIFICATION/DOWNGRADING SCHEDULE

16. DISTRIBUTION STATEMENT (of this Report)

Approved for public release; distribution unlimited.

17. DISTRIBUTION STATEMENT (of the abstract entered in Block 20, if different from Report)

18. SUPPLEMENTARY NOTES

19. KEY WORDS (Continue on reverse side if necessary and identify by block number)

Sun
Corona
Interplanetary Magnetic Field
Solar Physics

20. ABSTRACT (Continue on reverse side if necessary and identify by block number)

Previous global models of coronal magnetic fields have used a geometrical construction based on a spherical source surface because of requirements for computational speed. As a result they have had difficulty accounting for (a) the tendency of full magnetohydrodynamic (MHD) models to predict non-radial plasma flow out to r ~ 10 $r_\odot$ and (b) the appreciable magnitude, (~3γ, about 3 gamma) of B_r (the radial component of B) consistently observed at r ~ 1 AU. We present a new modelling technique based on a nonspherical source surface,

about 10 solar radii

about 4B

next page

DD FORM (FACSIMILE) 1473

409 944

UNCLASSIFIED

SECURITY CLASSIFICATION OF THIS PAGE (When Data Entered)

19. KEY WORDS (Continued)

20. ABSTRACT (Continued)

is presented which is taken to be an isogauss of the underlying potential field generated by currents in or below the photosphere. This modification of the source surface significantly improves the agreement between the geometrical construction and the MHD solution while retaining most of the computational ease provided by a spherical source surface. A detailed comparison between the present source-surface model and the MHD solution is made for the internal dipole case. The resulting B field agrees well in magnitude and direction with the coronal B field derived from the full MHD equations. It shows evidence of the slightly equatorward meridional plasma flow that is characteristic of the MHD solution. Moreover, the B field obtained by using our nonspherical source surface agrees well with that observed by spacecraft in the vicinity of the earth's orbit. Applied to a solar dipole field with a moment of 1 G-$r_\odot^3$, the present model predicts that B_r at $r \sim 1$ AU lies in the range of $\sim 1 - 2\gamma$ and is remarkably insensitive to heliocentric latitude. Very close to the neutral sheet B_r rises to a maximum value of $\sim 6\gamma$. Isogauss surfaces for two representative solar rotations are calculated from expansions of observed photospheric magnetic field data, and it is shown that deviations from sphericity of these surfaces are large and significant.

PREFACE

The authors are pleased to thank Dr. G. W. Pneuman for supplying a numerical description of the MHD results for the dipole case and for sending us recent preprints on the subject of coronal-field modelling. We are grateful to Dr. M. D. Altschuler and Dr. R. H. Levine for supplying sets of spherical-harmonic expansion coefficients (g_n^m and h_n^m) corresponding to selected solar rotations. Finally, we are pleased to thank Dr. H. H. Hilton for computing the isogauss contours at selected longitudes from the above-mentioned sets of expansion coefficients and Prof. C. F. Kennel for making helpful comments on the final form of the manuscript.

This work was supported in part by the company-financed research program of The Aerospace Corporation and in part by U.S. Air Force Space and Missile Systems Organization (SAMSO) contract F04701-77-C-0078.

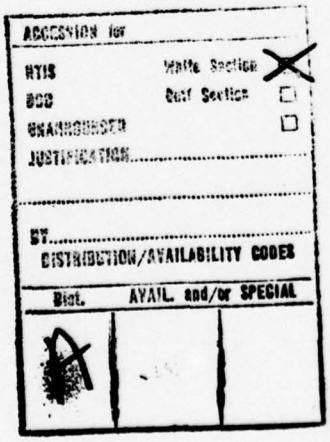

CONTENTS

TABLES

FIGURES

FIGURES (Continued)

1. INTRODUCTION

The purpose of this work is to describe a straightforward geometrical construction that approximates the mapping of solar magnetic fields through the corona to interplanetary space. The construction is based conceptually on the source-surface model introduced by Schatten et al. (1969) and by Altschuler and Newkirk (1969). The source surface in their models is a sphere of radius $r_s = 1.6\text{-}2.5\ r_\odot$ (solar radii) on which the scalar potential V (from which $\underset{\sim}{B} = -\underset{\sim}{\nabla} V$ is derived for $r \leq r_s$) is made constant. This constraint has the effect of making $\underset{\sim}{B}$ radial at $r = r_s$. The field outside the source surface in their models is generated from the spiral-field construction of Parker (1958) by imposing the continuity of $\underset{\sim}{B}$ at $r = r_s$.

The traditional source-surface models (Schatten et al., 1969; Altschuler and Newkirk, 1969) are computationally very simple and yield a qualitatively pleasing reproduction of major heliomagnetic features such as helmet streamers, filaments, arcades of closed field lines, and coronal holes. However, these models are only approximations to a rigorous magnetohydrodynamic (MHD) solution of the interaction between the solar wind and the coronal magnetic field. The inaccuracy inherent in these models prevents a detailed comparison of magnetic structures in the outer corona and solar wind with observed magnetic field patterns in the photosphere. The major weakness in these models is the incompatibility of the postulated radial magnetic field with MHD at $r \lesssim 10\ r_\odot$. This weakness is well illustrated by comparison with the only existing MHD solution (Pneuman and Kopp, 1971a,b), which was obtained for the special case in which the normal component of the photospheric field is that of a dipole field

with a polar field strength of 1 G. In Figure 1 the usual source-surface solution for this case is compared with the MHD solution. The differences are quite obvious. The MHD field lines are not even approximately radial for $r > r_s = 2.5\ r_\odot$, and the choice of a smaller source surface would make the disagreement even worse.

There have been subsequent attempts to replace the source-surface models by models which represent the MHD effects more accurately. Schatten (1971) developed an analytical technique that was based on the idea of placing sheet currents between oppositely directed open field lines. The resulting construction produced a qualitative improvement, in that the open field lines were indeed deflected equatorward instead of being radial; however, field lines in the region near the cusps of helmet streamers were poorly modelled thereby. (In order to model well the direction of the open field lines, the cusps had to be placed unrealistically low, i.e., at $1.6\ r_\odot$ in the dipole case.) Yeh and Pneuman (1977) developed a much more rigorous sheet-current model in which the location and strengths of current sheets between oppositely directed open field lines (and between closed and open structures) are actually calculated iteratively by determining the force balance between the magnetic field and the gas pressure in the expanding corona. Their result was shown to be very accurate when compared with the MHD dipole solution, but the calculation was so lengthy that it appears impractical to generalize their scheme to the point of applying it to a set of observed photospheric magnetic fields.

In the present work we develop a construction that retains most of the computational simplicity of the earlier source-surface models but which significantly improves the agreement with the MHD solution in the dipole case. We do this by adopting an

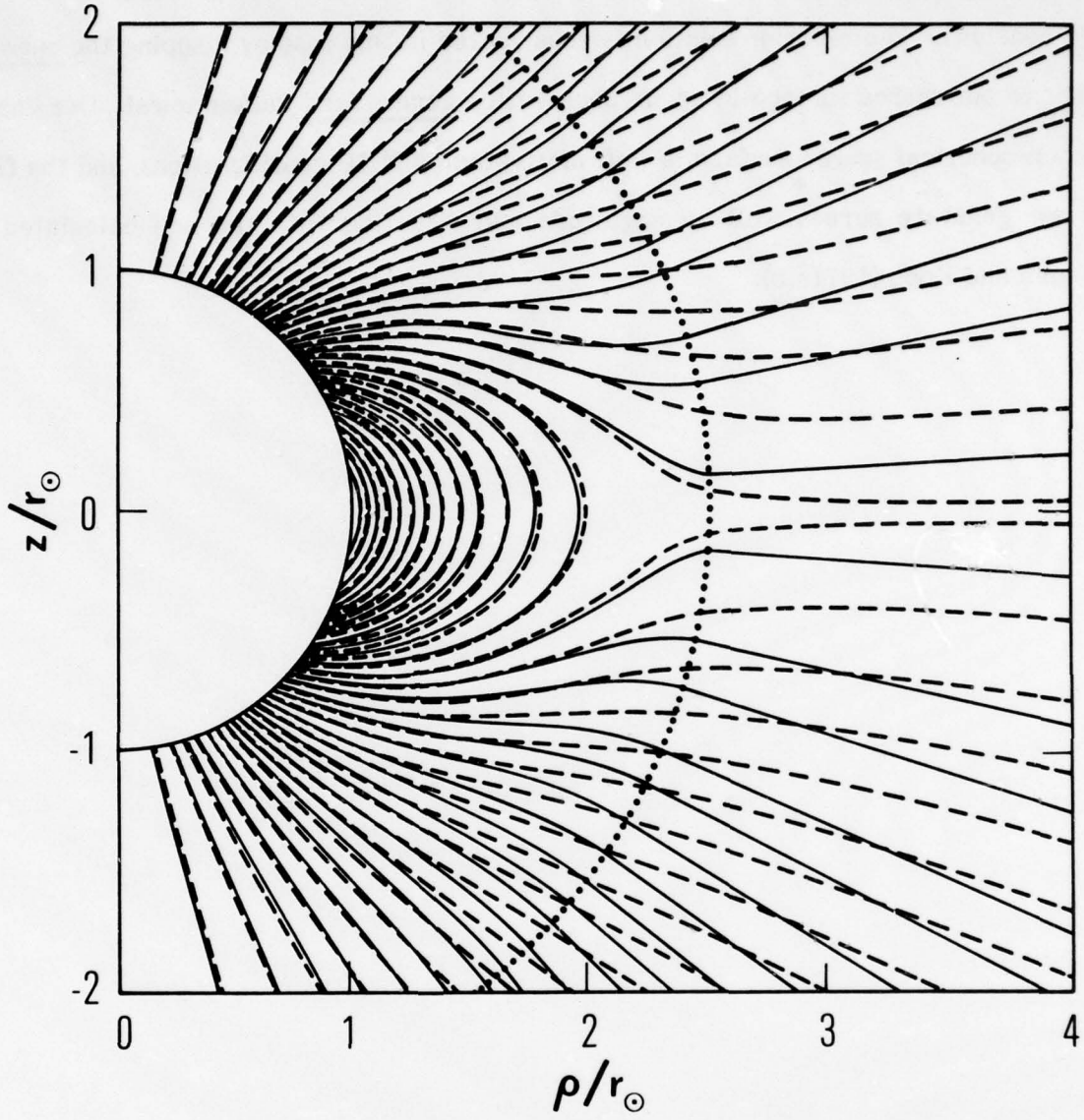

Fig. 1. Configuration of Magnetic Field Lines Emanating from an Internal Solar Dipole in the MHD Solution of Pneuman and Kopp (1971a, b; dashed curves) and in the Source-Surface Model of Altschuler and Newkirk (1969; solid curves). The spherical source surface (dotted curve) was taken to have a radius equal to 2.5 $r_\odot$ (Altschuler and Newkirk, 1969).

appropriate non-spherical source surface on which the heliomagnetic scalar potential V is made constant. The exterior solution is constructed in this case by mapping the outward normal to our source surface in accordance with a generalized Parker spiral. Our choice of a non-spherical source surface is well motivated by MHD considerations, and the field that we generate agrees well in magnitude and direction with the one calculated by Pneuman and Kopp (1971a,b).

2. NONSPHERICAL SOURCE SURFACE

For our non-spherical source surface, we select an appropriate isogauss of the spherical-harmonic extrapolation of the magnetic field derived from internal sources, i.e., without considering the effects of currents external to the sun. The identification of the source surface with an isogauss rather than a sphere represents a better simulation of magnetohydrohynamic (MHD) behavior. One should expect the magnetic field to be distorted very little by plasma currents where B is large, but very much where B is small. Thus, the influence of the solar dipole should be relatively less perturbed by plasma currents at polar latitudes than at equatorial, for observers stationed at the same heliocentric distance.

We do not attempt to specify the source surface self-consistently, e.g., by including the effects of external currents on $\underset{\sim}{B}$, and therefore on the shape of the critical isogauss. We are not attempting here to solve a problem in MHD rigorously, but are instead trying to formulate a straightforward geometrical construction. The accuracy of our construction is easily tested by comparing our results with an MHD solution, and our model is amply vindicated by such a comparison.

After the non-spherical source surface $r_s(\theta, \varphi)$ is identified from the spherical-harmonic expansion deduced from the observed photospheric magnetic field, the coronal field interior to the source surface is derived under the assumption that this volume is current-free. The coronal $\underset{\sim}{B}$ field there is calculated from a scalar potential of the form

$$V = r_\odot \sum_{n=1}^{N} \sum_{m=0}^{n} [(r_\odot/r)^{n+1} (g_n^m \cos m\varphi + h_n^m \sin m\varphi) P_n^m(\theta)$$

$$+ (r_0/r_\odot)(r/r_0)^n (\bar{g}_n^m \cos m\varphi + \bar{h}_n^m \sin m\varphi) P_n^m(\theta)], \quad (1)$$

where r_0 is a (constant) radius representative of the non-spherical source surface. In the dipole solution that follows, the parameter r_0 is the equatorial radius of the source surface. In a general solution, r_0 is merely a parameter that conveniently represents the particular isogauss level that is chosen. For example, one might identify the critical isogauss either by specifying B_0 (the value of $|\underset{\sim}{B}|$ on the surface) or by specifying

$$r_0/r_\odot \equiv B_0^{-1/3}[(g_1^0)^2 + (g_1^1)^2 + (h_1^1)^2]^{1/6} \quad (2)$$

as a general definition clearly consistent with (and, indeed, motivated by) the dipole case. The coefficients g_n^m and h_n^m are (of course) already determined from the spherical-harmonic expansion deduced from observations of photospheric field (e.g., Altschuler et al., 1977).

The coefficients $\bar{g}_n^m$ and $\bar{h}_n^m$ are chosen so as to minimize the mean-square tangential component of $\underset{\sim}{B}$ over the source surface. This is an operational way of saying that $\underset{\sim}{B}$ should be (as nearly as possible) normal to the source surface. This statement is a

straightforward generalization from the model characterized by a spherical source surface. There are two main complications in this generalization: There is no longer a simple relation between the $\bar{g}_n^m$ ($\bar{h}_n^m$) coefficients and the g_n^m (h_n^m) coefficients, and one cannot be assured that any spherical-harmonic potential exists that makes $\underset{\sim}{B}$ normal to the source surface over the entire area. We therefore ask only that the $\bar{g}_n^m$ and $\bar{h}_n^m$ coefficients be such as to minimize the integral

$$\sigma \equiv \oint B_t^2 \, dA \tag{3}$$

over the source surface, where B_t is the tangential component of $\underset{\sim}{B}$.

To obtain $\underset{\sim}{B}$ outside the non-spherical source surface, we construct the outward normal to the source surface and make the normal component of $\underset{\sim}{B}$ continuous there. This is an obvious generalization from the case of a spherical source surface. It should be quite effective when the source surface has a relatively simple shape, e.g., in the dipole case discussed in the following section. However, one may question this procedure for more complicated source surfaces, and one must recognize that the procedure becomes meaningless if the source surface is not everywhere convex. However, even in such extreme cases, the solution internal to the source surface might be utilized to prescribe a magnetic field geometry so that the hydrodynamic problem of coronal expansion within a specified field geometry can be solved (Durney and Pneuman, 1975). In such a case the external flow field might be obtained from hydrodynamics (rather than MHD) by imposing the Durney-Pneuman solution as a boundary condition at the non-spherical source surface. In essence, then, we specify a very simple extrapolation of the field normal to the source surface but recognize that a more realistic (albeit more complicated) solution might be necessary in practice.

3. THE DIPOLE CASE

The application of our technique to the case of an internal solar dipole is very instructive for several reasons. First, the source surface can be expressed analytically, so as to make the least-squares minimization of (3) particularly simple. This allows us to investigate the stability of the solution and the convergenge of the calculated $\bar{g}_n^0$ as N, the maximum allowed order, is increased. Second, the solution is directly comparable with the MHD dipole solution of Pneuman and Kopp (1971a,b). This comparison will be used as the primary test of the accuracy of our technique. Finally, even such a simple field configuration as the solar dipole already yields very instructive information about the behavior of the interplanetary $\underset{\sim}{B}$ field, as observed at $r \sim 1$ AU. Therefore, we present the detailed solution of the solar-dipole case to illustrate the advantages of a non-spherical source surface. The isogauss surfaces of a dipolar magnetic field have the general form

$$r = (1 + 3\cos^2\theta)^{1/6} r_0, \tag{4}$$

where r_0 is the equatorial radius and θ is the colatitude. For a 1-G polar field the choice $r_0 = 2.5\ r_\odot$ would correspond to a surface of constant $B \equiv |\underset{\sim}{B}| = 0.032$ G in the absence of external currents. It develops (see below) that an equatorial radius $r_0 = 2.3\ r_\odot$ provides a much better overall agreement between our model and the solution of Pneuman and Kopp (1971a,b). We remark parenthetically that the source surface described by (4) encloses a volume equal to $1.380173\ (4\pi/3) r_0^3$, and that a dipolar source surface of equatorial radius $r_0 = 2.245\ r_\odot$ would enclose the same volume as the spherical source surface (of radius $2.5\ r_\odot$) used by Altschuler and Newkirk (1969).

3.1 Internal Solution

In the dipole case, which is azimuthally symmetric, the scalar potential inside the source surface simplifies from (1) to the form

$$V = r_\odot g_1^0 (r_\odot/r)^2 \cos\theta + r_0 \sum_{n=1}^{N} (r/r_0)^n \bar{g}_n^0 P_n(\cos\theta), \qquad (5)$$

where the $\bar{g}_n^0$ are expansion coefficients to be determined below and the $P_n(\cos\theta)$ are Legendre polynomials. The term involving g_1^0 generates the field of the underlying internal dipole. The magnetic field $\underset{\sim}{B}$ (= $-\underset{\sim}{\nabla}V$) corresponding to (5) is given by

$$\underset{\sim}{B} = 2\hat{\underset{\sim}{r}} g_1^0 (r_\odot/r)^3 \cos\theta + \hat{\underset{\sim}{\theta}} g_1^0 (r_\odot/r)^3 \sin\theta$$

$$- \hat{\underset{\sim}{r}} \sum_{n=1}^{N} n (r/r_0)^{n-1} \bar{g}_n^0 P_n(\cos\theta)$$

$$+ \hat{\underset{\sim}{\theta}} \sum_{n=1}^{N} (r/r_0)^{n-1} \bar{g}_n^0 P_n'(\cos\theta) \sin\theta . \qquad (6)$$

The coefficients $\bar{g}_n^0$ are to be chosen so as to minimize σ, which is the integral of $B_t^2 \equiv (\hat{\underset{\sim}{n}} \times \underset{\sim}{B})^2$ over the surface defined by (4), where $\hat{\underset{\sim}{n}}$ is the unit vector in the direction of the outward normal to the source surface. In terms of (4) this means that $\hat{\underset{\sim}{n}}$ is the unit vector in the direction of $\underset{\sim}{\nabla} r_0(r, \theta)$:

$$\underset{\sim}{\hat{n}} = (1 + 7\cos^2\theta + 8\cos^4\theta)^{-1/2}\left[(1 + 3\cos^2\theta)\,\underset{\sim}{\hat{r}} + \underset{\sim}{\hat{\theta}}\sin\theta\cos\theta\right]. \qquad (7)$$

Thus, we seek to minimize the integral

$$\sigma \equiv \oint B_t^2\, dA \equiv \oint (\underset{\sim}{\hat{n}} \times \underset{\sim}{B})^2\, dA \qquad (8)$$

with respect to the $\bar{g}_n^0$, where

$$dA = 2\pi r \sin\theta \left[r^2 + (dr/d\theta)^2\right]^{1/2} d\theta$$

$$= 2\pi r_0 (1 + 7\cos^2\theta + 8\cos^4\theta)^{1/2} (1 + 3\cos^2\theta)^{-2/3} \sin\theta\, d\theta \qquad (9)$$

is the element of area on the source surface. Since the expansion coefficients $\bar{g}_n^0$ in (5) must vanish for even n in order to preserve the north-south symmetry of the $\underset{\sim}{B}$ field, it follows from (8) that

$$\sigma = 4\pi r_0^2 \int_0^1 (1 + 3x^2)^{-2/3} (1 + 7x^2 + 8x^4)^{1/2} B_t^2\, dx, \qquad (10)$$

where $x = \cos\theta$. Moreover, it follows from (6) and (7) that

$$B_t = (1 + 7x^2 + 8x^4)^{-1/2} (1 + 3x^2)^{-1/2} (1 - x^2)^{1/2}$$

$$\times \left\{ (r_\odot/r_0)^3 (1 + x^2)\ g_1^0 \right.$$

$$\left. + \sum_{n=1}^{N} (1 + 3x^2)^{(n+2)/6}\ \bar{g}_n^0 \left[nxP_n(x) + (1 + 3x^2)P_n'(x) \right] \right\}. \qquad (11)$$

We seek to minimize σ with respect to each of the expansion coefficients $\bar{g}_m^0$ by setting $\partial\sigma / \partial \bar{g}_m^0 = 0$. There follows from this condition the requirement that

$$\int_0^1 (1 + 7x^2 + 8x^4)^{-1/2} (1 + 3x^2)^{-5/3} (1 - x^2) (1 + 3x^2)^{(m+2)/6}$$

$$\times \left[mxP_m(x) + (1 + 3x^2)P_m'(x) \right] \left\{ (r_\odot/r_0)^3 (1 + x^2)\ g_1^0 \right. \qquad (12)$$

$$\left. + \sum_{n=1}^{N} (1 + 3x^2)^{(n+2)/6}\ \bar{g}_n^0 \left[nx\, P_n(x) + (1 + 3\,x^2)\, P_n'(x) \right] \right\} dx = 0$$

for every odd integer $m \leq N$. Thus, one must solve a set of simultaneous linear equations to determine the required coefficients $\bar{g}_n^0$. Our requirement can be expressed more concisely in matrix form. We require that

$$\sum_{n=1}^{N} (\bar{g}_n^0/g_1^0)\ \Lambda_{nm} = -(r_\odot/r_0)^3\ K_m, \tag{13a}$$

where

$$\Lambda_{nm} = \int_0^1 (1 + 7x^2 + 8x^4)^{-1/2}\ (1 + 3x^2)^{(m+n-6)/6} (1 - x^2)$$

$$\times \left[(1 + 3x^2)\ P_n'(x) + nx\ P_n(x)\right]$$

$$\times \left[(1 + 3x^2)\ P_m'(x) + mx\ P_m(x)\right] dx \tag{13b}$$

and

$$K_m = \int_0^1 (1 + 7x^2 + 8x^4)^{-1/2}\ (1 + 3x^2)^{(m-8)/6}\ (1 - x^4)$$

$$\times \left[(1 + 3x^2)\ P_m'(x) + mx\ P_m(x)\right] dx \tag{13c}$$

for n,m = 1,3,5,7,. . . , N-2, N. The matrix Λ_{nm} is clearly symmetric, i.e., $\Lambda_{nm} = \Lambda_{mn}$. Therefore, one may alternatively view $\bar{g}_n^0/g_1^0$ as a column vector and express (13a) in the form

$$\sum_{n=1}^{N} \Lambda_{mn}\ (\bar{g}_n^0/g_1^0) = -(r_\odot/r_0)^3\ K_m, \tag{14}$$

where K_m is considered a column vector.

The least-squares condition that determines the $\bar{g}_n^0$ can thus be solved by standard matrix-inversion techniques. The array Λ_{mn} is very well conditioned, being nearly tri-diagonal. Away from the three main diagonals the array values decrease by approximately two orders of magnitude per diagonal. We have solved (14) for the $\bar{g}_n^0$ with N = 5,7,9,11,13,15. The results are shown in Table 1. It is quite evident from this tabulation that the results are well behaved, and that the expansion coefficients $\bar{g}_n^0$ converge rapidly to the values that they would acquire in the limit $N \longrightarrow \infty$.

Table 1. Optimal Values of $(r_0/r_\odot)^3 (\bar{g}_n^0/g_1^0)$ for Use in (5), as Determined by Minimizing the Value of σ Specified by (10).

n	N=5	N=7	N=9	N=11	N=13	N=15
1	-0.62917	-0.63124	-0.63185	-0.63205	-0.63211	-0.63213
3	+0.11960	+0.12537	+0.12716	+0.12775	+0.12795	+0.12802
5	-0.03038	-0.04088	-0.04448	-0.04574	-0.04619	-0.04635
7		+0.01086	+0.01607	+0.01820	+0.01903	+0.01935
9			-0.00418	-0.00674	-0.00795	-0.00847
11				+0.00168	+0.00293	+0.00360
13					-0.00069	-0.00130
15						+0.00029

3.2 Exterior Solution

The meridional component of $\underset{\sim}{B}$ at $r > (1 + 3\cos^2\theta)^{1/6} r_0$ in the present model is defined by constructing the outward normal to the source surface, i.e., by constructing a straight line parallel to the unit vector $\hat{\underset{\sim}{n}}$ specified by (7). In view of the azimuthal symmetry of the dipole problem, it proves convenient to introduce the cylindrical coordinates $\rho = r \sin\theta$ and $z = r\cos\theta$. Since $\hat{\underset{\sim}{r}} = \hat{\underset{\sim}{\rho}} \sin\theta + \hat{\underset{\sim}{z}} \cos\theta$ and $\hat{\underset{\sim}{\theta}} = \hat{\underset{\sim}{\rho}} \cos\theta - \hat{\underset{\sim}{z}} \sin\theta$, it follows from (7) that

$$\hat{\underset{\sim}{n}} = (1 + 7\cos^2\theta + 8\cos^4\theta)^{-1/2} \left[(1 + 4\cos^2\theta)\, \hat{\underset{\sim}{\rho}} \sin\theta + 4\, \hat{\underset{\sim}{z}} \cos^3\theta\right] . \qquad (15)$$

Thus, the outward normal to the source surface at colatitude θ_s is a straight line having the slope

$$dz/d\rho = 4(1 + 4\cos^2\theta_s)^{-1} \cos^2\theta_s \operatorname{ctn}\theta_s \qquad (16)$$

and the intercepts

$$\rho_s = r_0 (1 + 3\cos^2\theta_s)^{1/6} \sin\theta_s \qquad (17a)$$

$$z_s = r_0 (1 + 3\cos^2\theta_s)^{1/6} \cos\theta_s . \qquad (17b)$$

3.3 Comparison with MHD Solution

In Figure 2, the interior and exterior solutions are joined at $r = (1 + 3 \cos^2 \theta)^{1/6} r_0$ and are compared with the MHD solution. The footpoints of the field lines were chosen to coincide with those in the figure published by Pneuman and Kopp (1971a,b). A reasonable match to the overall configuration of field lines is achieved with $r_0 = 2.3\ r_\odot$. The improvement of the present model, with its non-spherical source surface, over models with spherical source surfaces can be seen by comparing Figure 2 with Figure 1. The direction of the field lines in the exterior region is improved dramatically. Even the shape of the field lines interior to the source surface is considerably improved. On the basis of this test with the dipole case, one would expect the present technique not only to allow a much more accurate comparison of observed interplanetary fields with photospheric fields, but also to model coronal structures more faithfully.

As has been stated before, the parameter r_0 is adjustable. It is not surprising that our good overall fit to the MHD solution requires $r_0 = 2.3\ r_\odot$, whereas the equatorial cusp of the MHD solution occurs at $r \approx 2.5\ r_\odot$. One could not expect our source-surface model to agree with the MHD solution in every detail. Thus, the construction of a realistic coronal-field model requires a certain degree of judgment in the selection of r_0, just as the selection of a radius for the spherical source surface has required in the past. Of course, the parameter r_0 can be adjusted to match specific features of the MHD solution very well. Figure 3 illustrates two such adjustments of r_0: the first to match the MHD solution in the region close to the neutral sheet, and the second to provide an explicit tracing of the cusped field line.

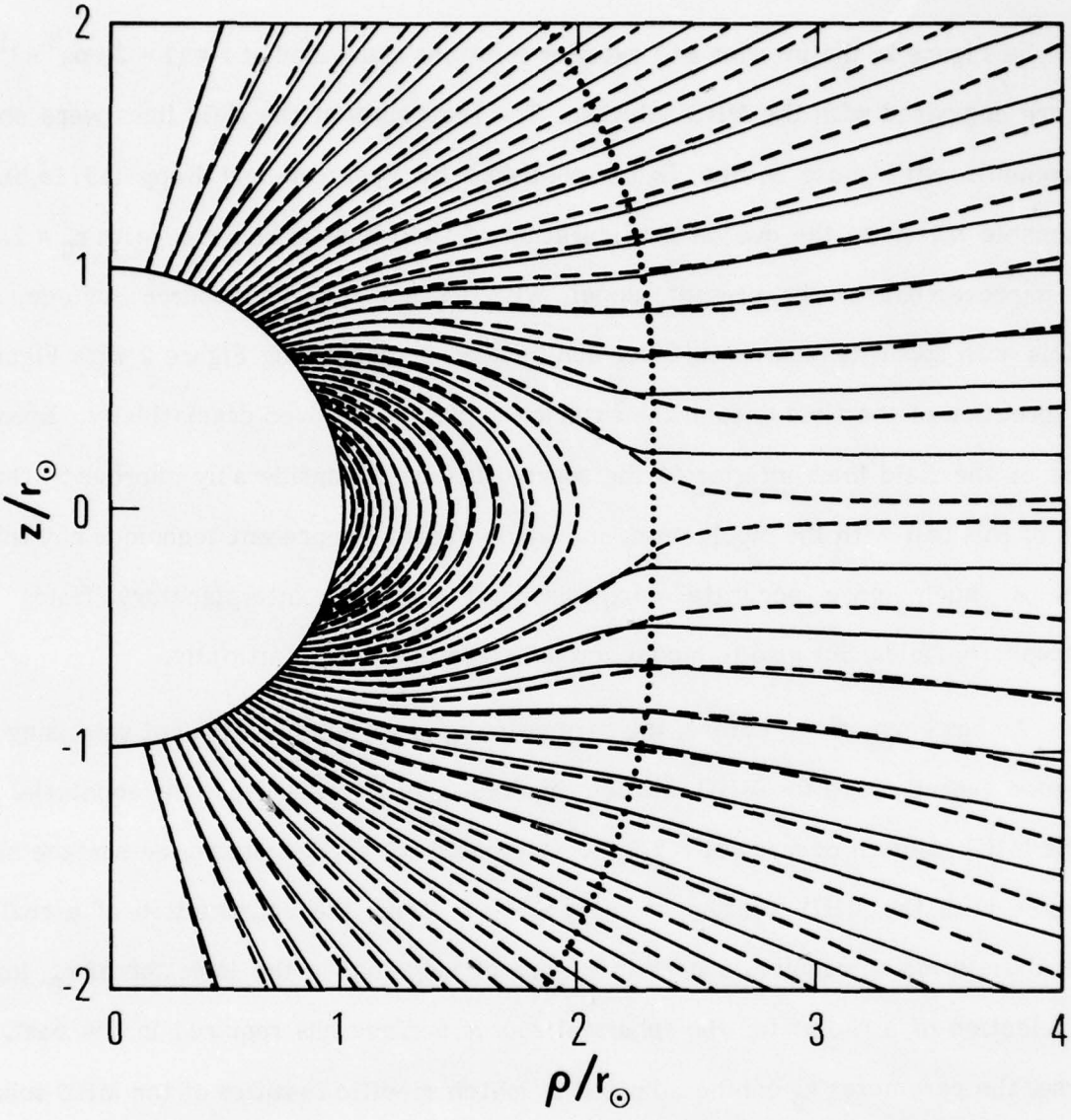

Fig. 2. Configuration of Magnetic Field Lines Emanating from an Internal Solar Dipole in the MHD Solution of Pneuman and Kopp (1971a, b; dashed curves) and in Our Source-Surface Model (solid curves). Our nonspherical source surface (dotted curve) is taken to have an equatorial radius $r_0 = 2.3\ r_\odot$, which corresponds to a polar radius $2^{1/3} r_0 \approx 2.9\ r_\odot$ (cf. Fig. 1). We have taken N = 15 in (5).

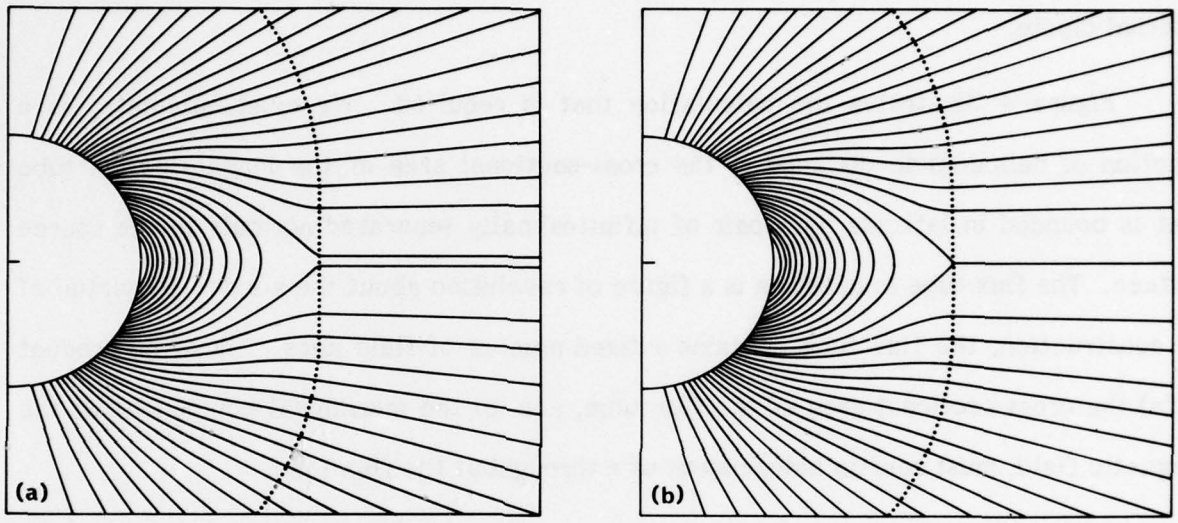

Fig. 3. Configuration of Magnetic Field Lines Emanating from an Internal Solar Dipole in Our Source-Surface Model for Selected Equatorial Radii $r_0 > 2.3\ r_\odot$: (a) to Match the Lowest-Latitude Open Field Lines Shown by Pneuman and Kopp (1971a, b) at $3\ r_\odot \lesssim r \lesssim 4\ r_\odot$, $r_0 = 2.3380\ r_\odot$; and (b) to Illustrate the Cusped Field Line Explicitly, $r_0 = 2.3391\ r_\odot$. As in Figs. 1 and 2, the illustrated field lines from the source-surface model were chosen so as to intersect the sun ($r = r_\odot$) at the same set of colatitudes $\theta_\odot$ as the MHD field lines plotted by Pneuman and Kopp (1971a, b). We have taken $N = 15$ in (5).

3.4 Interplanetary Magnetic Field

The present model yields a calculable interplanetary magnetic field that can be compared with spacecraft observations. This circumstance provides a further test of the accuracy of the model and allows for instructive predictions about the overall structure of the interplanetary $\underset{\sim}{B}$ field. Detailed calculations are provided here for the case of an internal dipole.

Figure 4 illustrates the calculation that is required. We must calculate, as a function of heliocentric distance r, the cross-sectional area of the magnetic flux tube that is bounded in latitude by a pair of infinitesimally separated normals to the source surface. The flux tube in question is a figure of revolution about the z axis. By virtue of its construction, the flux tube contains a fixed number of field lines. Thus, the product of (a) the cross-sectional area of the flux tube, and (b) the meridional component of the magnetic field, must remain independent of r throughout the flux tube.

The element of area transverse to the flux tube is given by $dA = 2\pi \rho \, ds_\perp$, where $ds_\perp$ is the thickness of the flux tube at heliocentric distance $r = \rho \csc \theta$. However, the thickness $ds_\perp$ at (r, θ, φ) is proportional to the distance of the point (r, θ, φ) from the center of curvature (C) of the source surface for the point $(r_s, \theta_s, \varphi_s)$ along the same normal (see Figure 4). Thus, if R is the radius of curvature at $(r_s, \theta_s, \varphi_s)$, the value of $ds_\perp$ is proportional to $R + \delta$, where δ is distance from $(r_s, \theta_s, \varphi_s)$ to (r, θ, φ). Therefore, the meridional component B_m of $\underset{\sim}{B}$ at (r, θ, φ) is related to the normal component B_s of $\underset{\sim}{B}$ at $(r_s, \theta_s, \varphi_s)$ by the formula

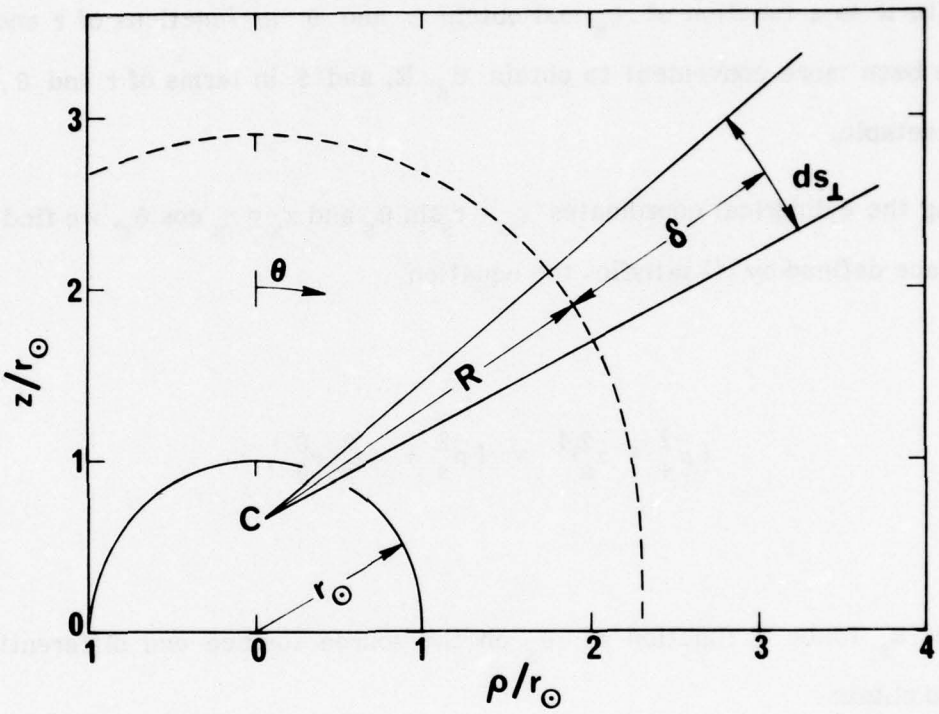

Fig. 4. Geometry of Meridional Cross Section of Magnetic Flux Tube (bounded by solid lines that intersect at C), as Employed in the Calculation of B at Points (r, θ) Outside Our Nonspherical Source Surface (dashed curve) From the Normal Component ($B_s \equiv \hat{n} \cdot B$) of B at the Source Surface

$$B_m = (\rho_s/\rho)\,[R/(R+\delta)]B_s$$

$$= (r_0/r)(\sin\theta_s/\sin\theta)\,[1 + (\delta/R)]^{-1}(1 + 3\cos^2\theta_s)^{1/6}\,B_s \qquad (18)$$

We calculate R as a function of θ_s and obtain δ and θ as functions of r and θ_s. It would have been more convenient to obtain θ_s, R, and δ in terms of r and θ, but this proved intractable.

Using the cylindrical coordinates $\rho_s = r_s \sin\theta_s$ and $z_s = r_s \cos\theta_s$, we find that the source surface defined by (4) satisfies the equation

$$(\rho_s^2 + z_s^2)^4 = (\rho_s^2 + 4z_s^2)\,r_0^6 \,. \qquad (19)$$

We consider z_s to be a function of ρ_s on the source surface and differentiate (19) implicitly to obtain

$$z_s' = -\frac{1}{4}(1 + 4\cos^2\theta_s)\sec^3\theta_s \sin\theta_s \qquad (20a)$$

$$z_s'' = -(1/8\,z_s)\,[(1 + 3\cos^2\theta_s)\sec^6\theta_s \sin^2\theta_s$$

$$+ 8 + 2\sec^2\theta_s + 8(z_s')^2\,]. \qquad (20b)$$

The radius of curvature is thereupon given (e.g., Thomas, 1960) by

$$R = |z_s''|^{-1} \left[1 + (z_s')^2 \right]^{3/2} . \qquad (21)$$

We note in particular that $R \to \infty$ at the equator ($\theta_s = \pi/2$) and that $R = 0.8\, r_s$ at the poles.

Since z_s' is the slope of the source surface, the equation

$$\rho - \rho_s = -(z - z_s)\, z_s' \qquad (22)$$

characterizes the normal to the source surface. Therefore, the normal distance δ of the point (r, θ, φ) from the source surface is given by

$$\delta \equiv \left[(\rho - \rho_s)^2 + (z - z_s)^2 \right]^{1/2} = \left[1 + (z_s')^2 \right]^{1/2} |z - z_s|$$

$$= \left[1 + (z_s')^2 \right]^{1/2} (z - z_s) \operatorname{sgn} (\cos \theta_s) . \qquad (23)$$

The remaining task is to calculate $z - z_s$ in terms of r and θ_s. To do this we write

$$r^2 = \rho^2 + z^2 = (\rho - \rho_s + \rho_s)^2 + (z - z_s + z_s)^2$$

$$= (\rho - \rho_s)^2 + (z - z_s)^2 + r_s^2 + 2\rho_s (\rho - \rho_s) + 2 z_s (z - z_s) \qquad (24)$$

and eliminate $(\rho - \rho_s)$ with the aid of (22). The result is a quadratic equation in $(z - z_s)$ that yields two solutions, one of which can be identified as extraneous because it fails to reduce to $z - z_s = (r - r_s)\,\mathrm{sgn}\,(\cos\theta_s)$ at $\cos\theta_s = \pm 1$ (i.e., at the poles). The acceptable solution reads

$$4\left[1 + (z_s')^2\right](z - z_s) =$$

$$\left\{16\left[1 + (z_s')^2\right](r^2 - r_s^2) + r_s^2(1 + 3\cos^2\theta_s)^2 \sec^6\theta_s\right\}^{1/2} \mathrm{sgn}\,(\cos\theta_s)$$

$$- r_s(1 + 3\cos^2\theta_s)\sec^3\theta_s, \qquad (25)$$

where $r_s = (1 + 3\cos^2\theta_s)^{1/6} r_0$ as usual. The substitution of (25) in (23) yields δ as a function of r and θ_s for fixed r_0. Moreover, it follows from (23) that

$$\cos\theta = (r_0/r)(1 + 3\cos^2\theta_s)^{1/6}\cos\theta_s$$

$$+ \left[1 + (z_s')^2\right]^{-1/2}(\delta/r)\,\mathrm{sgn}\,(\cos\theta_s), \qquad (26)$$

i.e., that θ can be written explicitly as a function of r and θ_s for fixed r_0.

We identify B_s in (18) with the normal component of $\underset{\sim}{B} = -\underset{\sim}{\nabla} V$ at the source surface:

$$B_s = (1 + 7\cos^2\theta_s + 8\cos^4\theta_s)^{-1/2}\left[(1 + 3\cos^2\theta_s)\,B_r + \sin\theta_s\cos\theta_s\,B_\theta\right]. \quad (27)$$

In order to facilitate applications of the present model by the interested reader, we present (in Table 2) listings of the quantity $(r_0/r_\odot)^3\,(B_s/g_1^0)\sec\theta_s$ as a function of $\cos\theta_s$ at the source surface for selected values of N in (5). We have selected this particular combination of variables because of the fact that its limit remains finite (and independent of $r_0/r_\odot$) as one approaches the equator ($\theta = \pi/2$), i.e., because $B_s \propto (r_\odot/r_0)^3\,g_1^0\cos\theta_s$ in this limit. The expression for B_m given by (18) becomes indeterminate at $\cos\theta = \pm 1$, i.e., at the poles. Since we find $z_s' = 0$ and (therefore) $R = |z_s''|^{-1} = 0.8\,r_s$ at $\cos\theta_s = \pm 1$, the correct limit for (18) is obtained by considering a spherical expansion from the center of curvature, which is located on the axis of symmetry at $z = 0.2\,r_s\,\mathrm{sgn}(\cos\theta)$. Thus, we obtain

$$B_m = B_r = 16\left[5(r/r_s) - 1\right]^{-2} B_s \quad (28)$$

at $\cos\theta = \pm 1$. The source-surface radius at the poles is given by $r_s = 2^{1/3}\,r_0$, according to (4). Since $B_\rho/B_z = -z_s'$ along the entire field line, it is easy enough to reconstruct $\underset{\sim}{B}$ in cylindrical (ρ, φ, z) or spherical coordinates outside the source surface:

Table 2. Values of $(r_0/r_\odot)^3 (\hat{n}\cdot\underset{\sim}{B}/g_1^0) \sec\theta_s$ at the Nonspherical Source Surface Given by (4), as Computed from (5) with the Optimal Coefficients $\overline{g}_n^0$ Specified in Table 1*

$\cos\theta_s$	N=5	N=7	N=9	N=11	N=13	N=15
0.0	3.452	3.745	3.960	4.113	4.222	4.300
0.1	3.396	3.674	3.873	4.009	4.101	4.164
0.2	3.243	3.479	3.629	3.717	3.766	3.792
0.3	3.028	3.193	3.269	3.293	3.291	3.281
0.4	2.773	2.844	2.840	2.809	2.781	2.765
0.5	2.484	2.459	2.401	2.362	2.352	2.358
0.6	2.171	2.082	2.032	2.034	2.053	2.063
0.7	1.853	1.773	1.787	1.819	1.823	1.810
0.8	1.572	1.585	1.634	1.624	1.607	1.611
0.9	1.400	1.489	1.455	1.444	1.463	1.455
1.0	1.442	1.245	1.376	1.289	1.346	1.312

*$B_s \equiv \hat{n}\cdot\underset{\sim}{B}$ at the source surface.

$$B_\rho = -\left[1 + (z_s')^2\right]^{-1/2} z_s' B_m \, \mathrm{sgn}(\cos\theta_s) \tag{29a}$$

$$B_z = \left[1 + (z_s')^2\right]^{-1/2} B_m \, \mathrm{sgn}(\cos\theta_s) \tag{29b}$$

$$B_r = \left[1 + (z_s')^2\right]^{-1/2} (\cos\theta - z_s' \sin\theta) B_m \, \mathrm{sgn}(\cos\theta_s) \tag{29c}$$

$$B_\theta = -\left[1 + (z_s')^2\right]^{-1/2} (\sin\theta + z_s' \cos\theta) B_m \, \mathrm{sgn}(\cos\theta_s) \tag{29d}$$

We assume that the sun rotates with angular velocity $\underset{\sim}{\Omega}$ about the dipole (z) axis and that the solar-wind velocity $\underset{\sim}{u}$ is directed along the normal to the source surface. Thus, we neglect the azimuthal component of $\underset{\sim}{u}$ while requiring that $u_\theta / u_r = B_\theta / B_r$. It follows from the argument offered by Parker (1958) that

$$B_\varphi = -(r \sin\theta - r_s \sin\theta_s)(\Omega / u) B_m \tag{30}$$

in our (more general) model. We would take $\Omega = 2.8925 \times 10^{-6}$ sec^{-1} in order to reproduce the 27-day periodicity of solar magnetic features observed from the orbiting earth (cf. Dessler, 1967). A simple model for B_φ could be constructed by adopting the nominal quiet-time solar-wind velocity (u = 320 km/sec) recommended by Hundhausen (1970), but a better model would require us instead to specify the probable variation of u with r and θ_s. Rather than burden the present work with a model for the solar-wind velocity, however, we shall ignore interplanetary comparisons of B_φ with that obtained from our model and concentrate instead of B_m.

Figure 5 illustrates the variation of B_m with $r/r_\odot$. In the left panel one follows a field line by holding fixed the value of θ_s (colatitude at which the field line intersects source surface) or, equivalently, of $\theta_\odot$ (colatitude at which the field line intersects the surface of the sun); in this case the latitude of evaluation decreases with increasing $r/r_\odot$. In the right panel one evaluates B_m at fixed latitude $\lambda \equiv |(\pi/2)-\theta|$. Thus, the left panel illustrates a conceptual point, while the right panel illustrates an observational one. Both panels illustrate a pronounced departure of $(r/r_\odot)^2 B_m$ from constancy at low latitudes, in marked contrast to the case of a spherical source surface. With a spherical source surface (Schatten et al., 1969; Altschuler and Newkirk, 1969) one would have obtained $\theta = \theta_s$, $B_\theta = 0$, and

$$B_r = 3 g_1^0 (r_\odot^3/r^2 r_s) \cos\theta , \qquad (31)$$

with r_s independent of θ_s. It would follow from (31) that $(r/r_\odot)^2 B_m$, as well as θ, should remain constant along a field line. Moreover, it would seem from (31) that the equatorial current sheet at $\theta = \pi/2$ is not a sharply defined feature. The azimuthal (φ) component of the current density would be given by

$$J_\varphi = (c/4\pi)\,\hat{\varphi}\cdot\nabla\times B = (3c/4\pi r_s)(r_\odot/r)^3 g_1^0 \sin\theta \qquad (32)$$

in the case of a spherical source surface. This would represent a distribution of current having a full width of 120° (out of a possible 180°) at half maximum.

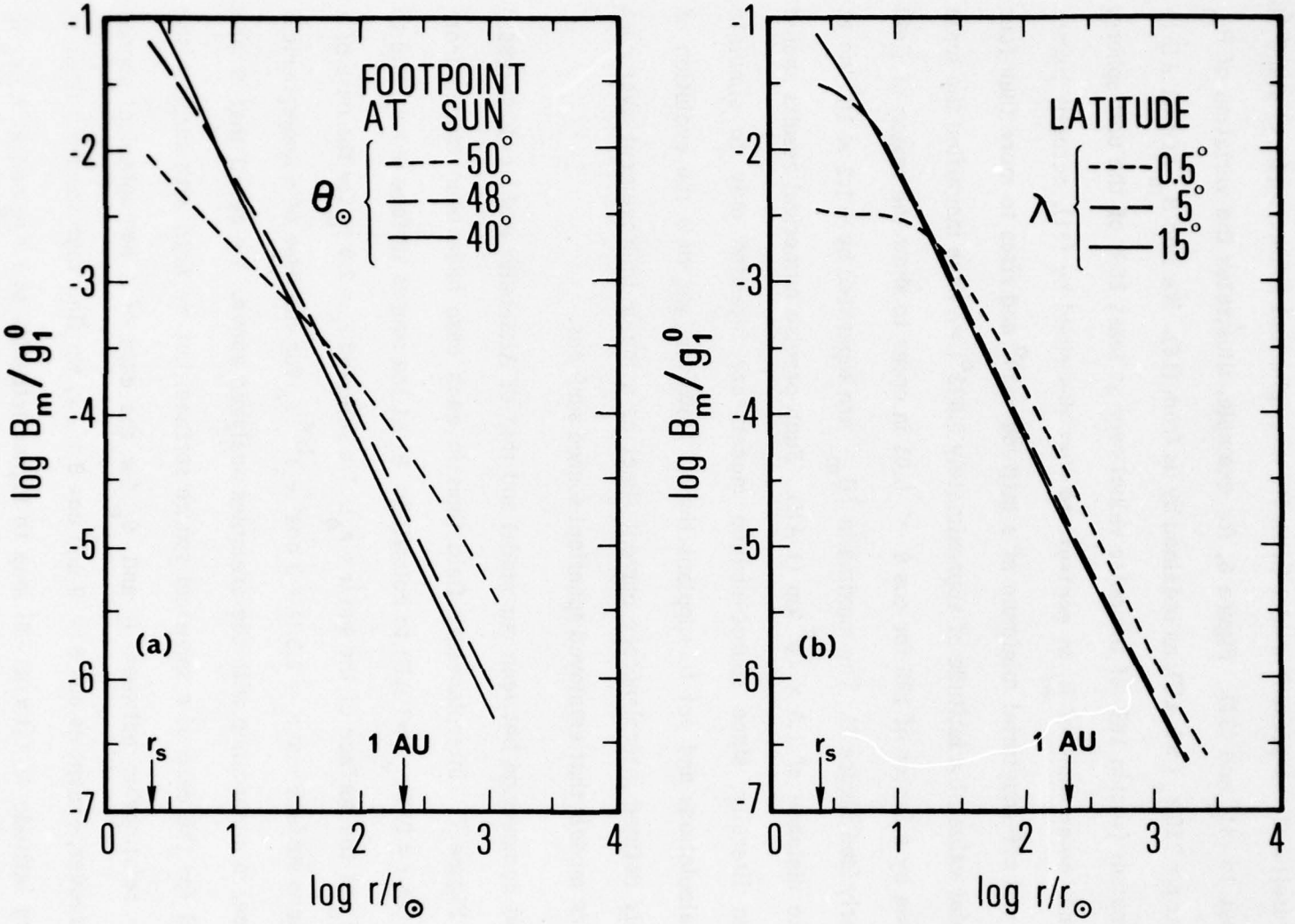

Fig. 5. Variation of Meridional Component B_m of Magnetic Field with Heliocentric Distance r Outside Our Nonspherical Source Surface of Equatorial Radius $r_0 = 2.3\ r_\odot$: (a) Along Selected Field Lines Identified by Their Colatitudes $\theta_\odot$ of Intersection with the Sun; and (b) at Selected Latitudes $\lambda\ |(\pi/2) - \theta|$. We have taken N = 15 in (5). variation of B_m with r is very nearly inverse-square for $\theta_\odot \lesssim 40^\circ$ in (a) and for $\lambda \gtrsim 15^\circ$ in (b).

The results of the present model (with its non-spherical source surface) stand in sharp contrast to (31) and (32). Figure 6, for example, illustrates the variation of B_m with cos θ at $r = 215\ r_\odot$ (≈ 1 AU), as obtained by us from (18). We find B_m at $r \approx 1$ AU to be nearly constant (within 10% of the polar value) over at least 85% of the unit sphere. Our meridional component of $\underset{\sim}{B}$, in contrast to that described by (31), actually passes through a broad off-equatorial minimum at a latitude $\sim 30^\circ$ and rises to more than four times the polar value at a latitude of approximately 0.023°; we have magnified the scale of the abscissa by a factor of 100 for cos θ < 0.01 in order to show the region of field reversal clearly (see Figure 6). The maxima in $|B_m|$ are separated by $\sim 1.2 \times 10^5$ km at a heliocentric distance of 1.5×10^8 km (1 AU). Such precise numerical results should not be taken literally, since source-surface models are intended only to simulate dynamical calculations and not to supplant them. However, we view the evolution of such a sharply defined interplanetary current sheet as a major improvement over past source-surface models that employed spherical source surfaces.

A final comparison between our model and that of Altschuler and Newkirk (1969) is shown in Figure 7. Interplanetary field lines in each case have been traced from colatitude θ at $r = 215\ r_\odot$ (≈ 1 AU) to colatitude θ_s at the source surface ($r = r_s$) and to colatitude $\theta_\odot$ at the surface of the sun ($r = r_\odot$). We selected $r_s = 2.5\ r_\odot$ for the case of a spherical source surface and $r_s = 2.3\ (1 + 3 \cos^2 \theta_s)^{1/6}\ r_\odot$ for the case of a non-spherical source surface, in accordance with the examples analyzed above. We recall that θ and θ_s are equal for the case of a spherical source surface, but we note with surprise the nearly linear relationship between θ and $\theta_\odot$ for the case of a non-spherical source surface. Moreover, except at cos $\theta = 0$ and cos $\theta = \pm 1$, we find that the field lines at interplanetary latitude $\lambda = |(\pi/2) - \theta|$ map to higher latitudes at $r = r_s$ and at $r = r_\odot$ in our model than in the model of Altschuler and Newkirk (1969).

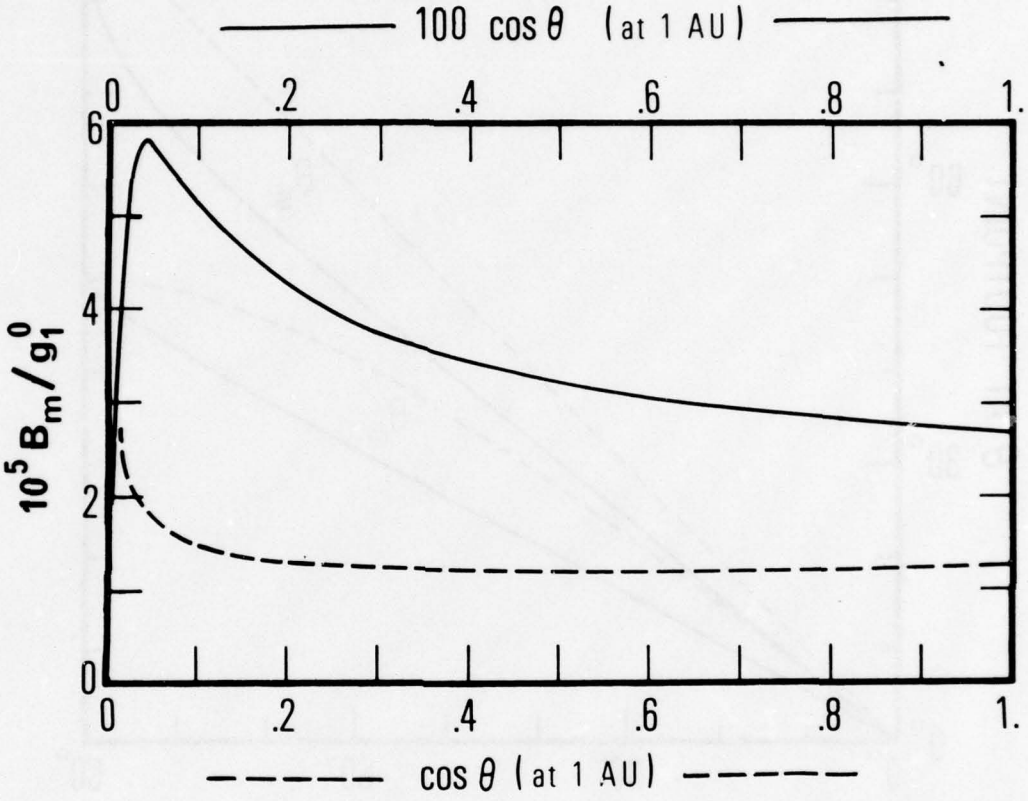

Fig. 6. Variation of Meridional Component B_m of Interplanetary Magnetic Field at Heliocentric Distance $r = 215\ r_\odot \approx 1$ AU with Colatitude θ for Nonspherical Source Surface with Equatorial Radius $r_0 = 2.3\ r_\odot$. Dashed curve and lower scale apply for $\cos\theta \geq 10^{-2}$; solid curve and upper scale apply for $\cos\theta \leq 10^{-2}$. We have taken $N = 15$ in (5). The ordinate measures B_m in γ($1\gamma \equiv 10^{-5}$ G) if one takes $g_1^0 = 1$ G.

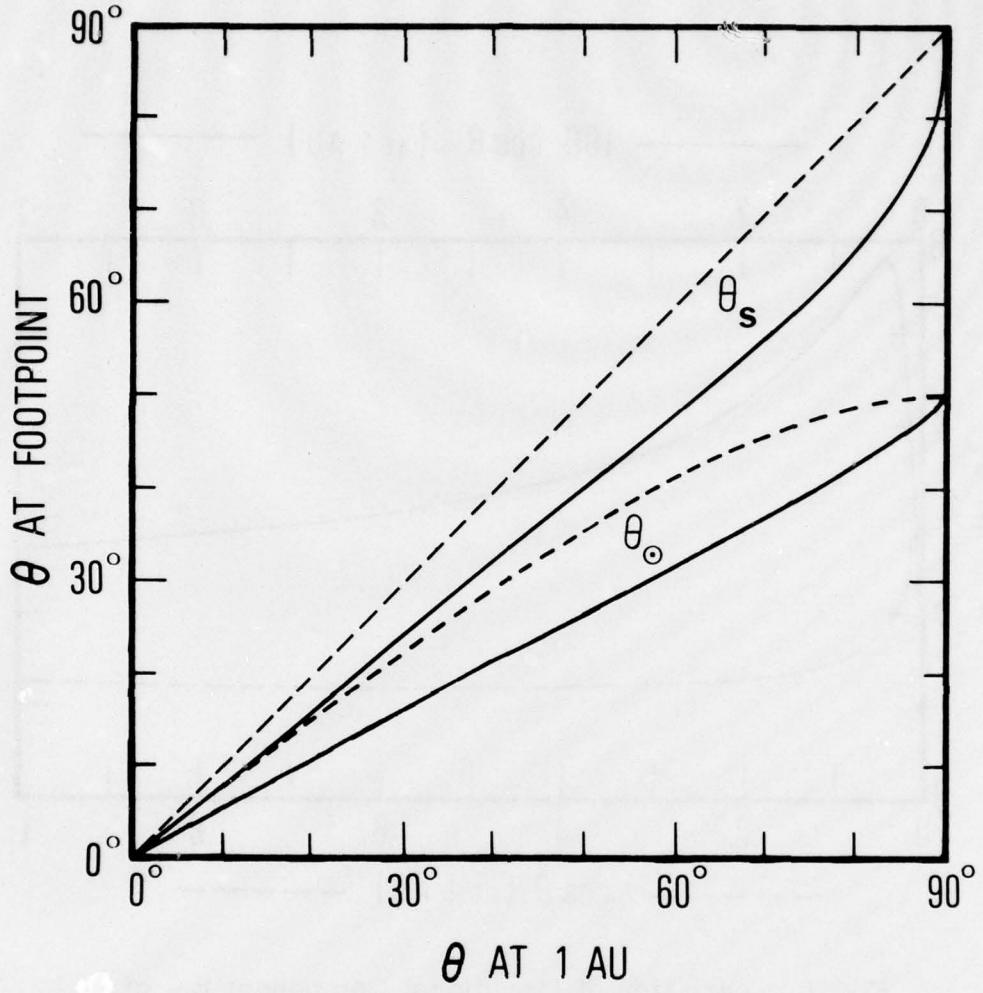

Fig. 7. Results of Tracing Magnetic Field Line from Colatitude θ at $r = 215\ r_\odot \approx 1$ AU in Interplanetary Space to Colatitude θ_s at the Source Surface ($r = r_s$) and Thence to Colatitude $\theta_\odot$ at the Surface of the Sun ($r = r_\odot$). Dashed curves correspond to the model of Altschuler and Newkirk (1969), i.e., to a spherical source surface of Radius $r_s = 2.5\ r_\odot$. Solid curves correspond to the present model, i.e., to a nonspherical source surface with equatorial radius $r_0 = 2.3\ r_\odot$. We have taken N = 15 in (5).

4. APPLICATION TO REALISTIC $\underset{\sim}{B}$ FIELD

The obvious extension of our concept of a non-spherical source surface is to apply it to the spherical-harmonic expansion deduced from a set of observed photospheric $\underset{\sim}{B}$-field data. This procedure carries the promise of allowing a calculation of realistic coronal and interplanetary magnetic fields that are accurate enough to permit a detailed investigation of a variety of solar-interplanetary structures, e.g., neutral sheets, sectors, high-speed streams, coronal holes, helmet streamers, and so on. In order to do this, one must develop a numerical program to minimize σ as given by (3) over an arbitrary, azimuthally asymmetric source surface. This is a rather large and complicated task, and is beyond the scope of the present paper. However, before such a task is started, we can and should investigate what the shape of a realistic source surface (as determined by the procedure outlined in Section 2) would be. Accordingly, we have obtained from R. H. Levine (personal communication, 1977) a set of spherical-harmonic expansion coefficients (g_n^m and h_n^m from n = 1 to n = 20, m = 0 to m = n) for use in (1) for two well-studied solar rotations (1602 and 1609). We have used these coefficients to calculate several isogauss surfaces. For purposes of illustration we have adopted the isogauss $|\underset{\sim}{B}|$ = 0.03 G as the hypothetical source surface. In accordance with the present prescription, the coefficients $\bar{g}_n^m$ and $\bar{h}_n^m$ in (1) have been neglected in calculating the isogauss.

The results are shown in Figure 8 in the form of synoptic contour plots of constant $r_s/r_\odot$. The actual shape of the isogauss surface for rotation 1602 can be seen more clearly in Figure 9, where two meridional cuts through the surface are shown. The

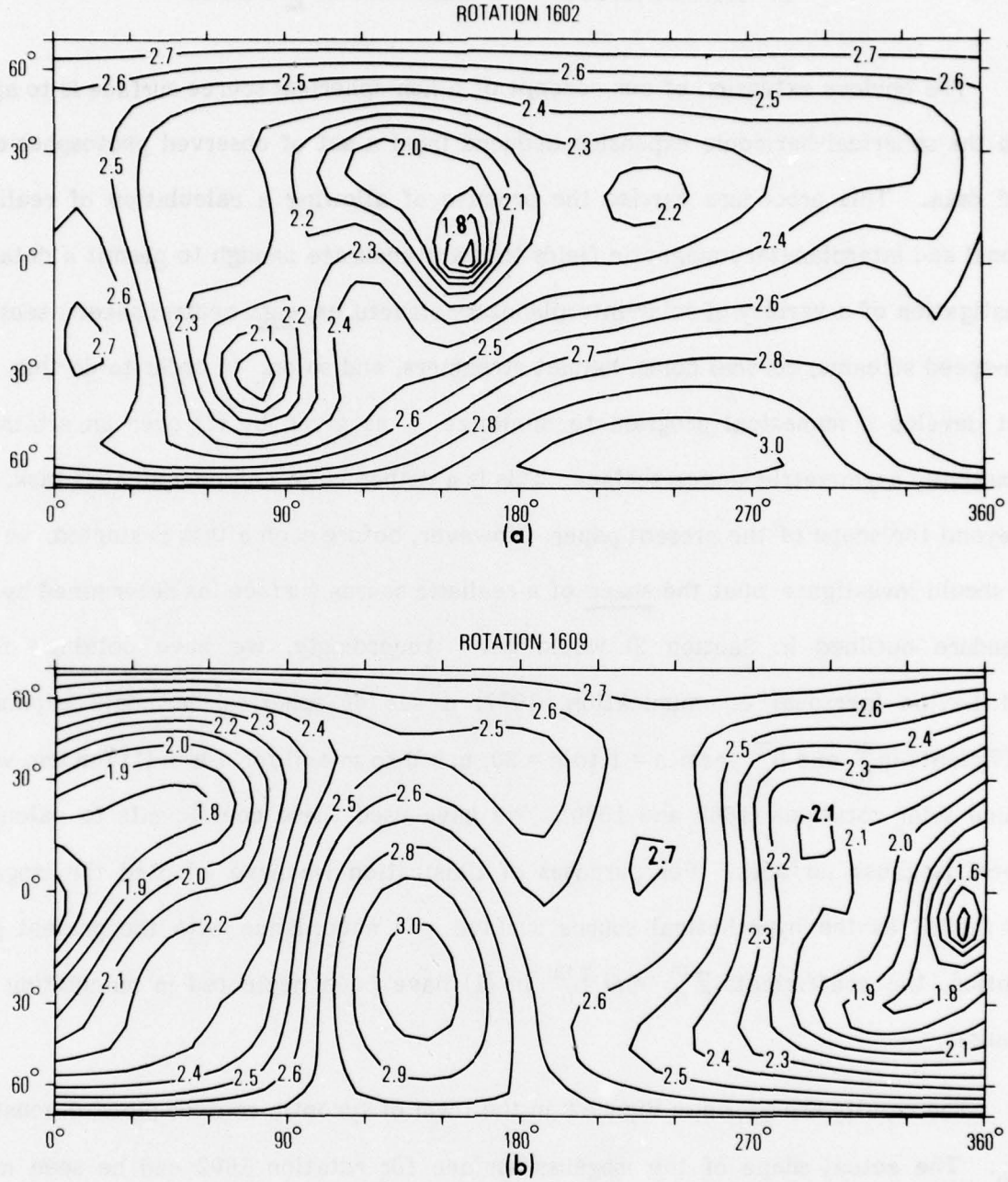

Fig. 8. Contours of Constant (specified) r_s/r_o on the Isogaussian "Source" Surface $|B| = 0.3$ G for Rotations 1602 (a) and 1609 (b), Based on (1) with (g_n^m, h_n^m) Supplied by R.H. Levine (personal communication, 1977) and (2) with $(\overline{g}_n^m, \overline{h}_n^m)$ Neglected

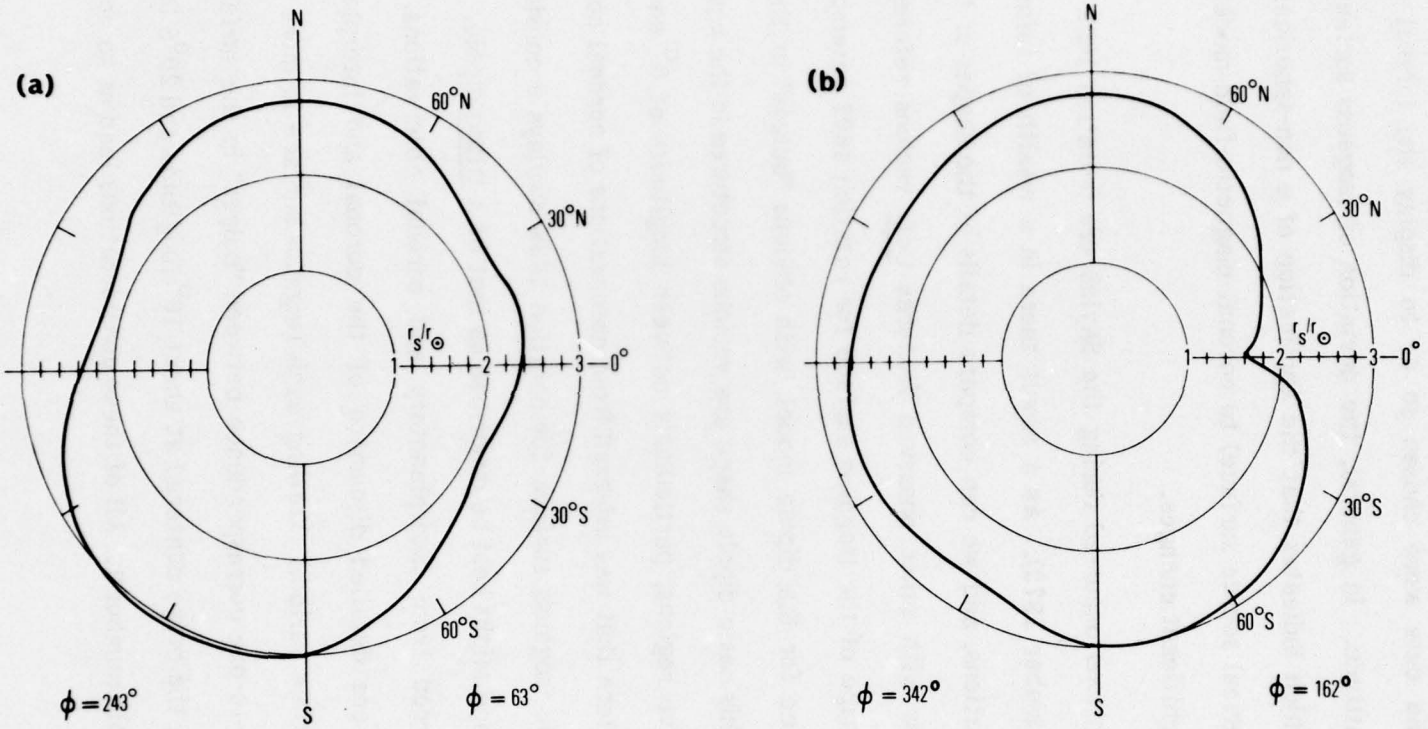

Fig 9. Meridional Cuts Showing $r_s/r_\odot$ as a Function of Latitude for the Isogauss $|B| = 0.3$ G on Rotation 1602. This representation accurately displays the shape of the isogauss source surface. These particular meridians were chosen to display the largest deviations of the source surface from sphericity.

particular longitudes of the cuts were chosen so as to display the largest possible variations of $r_s/r_\odot$ with latitude. In general, the deviation of isogauss surfaces from sphericity is very large, which indicates that the application of a non-spherical source surface (rather than a spherical source surface) to coronal magnetic-field models based on real data will produce significant changes.

The above solar rotations occurred during the Skylab era (rotation 1602 in June 1973; rotation 1609 in December 1973). As a result there is a wealth of information available for these two rotations, and we can compare details of the shapes of the corresponding isogauss surfaces with other observed features (cf. various references in Zirker, 1977). The basic shape of the isogauss surface for rotation 1602 resembles the shape of the isogauss surface for the dipole model, with obvious "bulges" in the polar regions. Superimposed on this basic dipole shape are various structures in the equatorial region associated with active regions, particularly between longitudes of 0° and 180°. This is the same general pattern that was inferred from observations of coronal holes and interplanetary streams. The isogauss surface for rotation 1609 displays a considerably different appearance; its shape might best be described as that of a tilted dipole. Again, this basic shape was inferred from interplanetary and coronal observations. (See Hundhausen, 1977, for a more detailed discussion of the coronal and interplanetary phenomenology during this time period.) Viewing each isogauss surface in more detail, we note that there is a one-to-one correspondence between "bulges" in the surface and coronal holes. For example, the bulge centered at about 10° longitude and 20°S latitude in rotation 1602 is coronal hole number 1. All of these considerations lead us to conclude

that the use of a non-spherical source surface would lead to a very significant improvement in current coronal field models.

The failure of a source surface to be everywhere convex entails no obvious impediment to the interior solution, i.e., to the minimization of σ in (3). However, this failure will definitely impact our construction of the exterior solution, since outward normals from different points on the source surface will necessarily intersect somewhere outside the source surface. Such intersections suggest the formation of shocks in the outer corona and perhaps correspond to features that are actually present in space. If confirmed by observation or by MHD theory, the presence of such shocks would be of interest in the context of heating the solar wind (C. F. Kennel, personal communication, 1978). However, since we do not know the fundamental relationship (if any) between source-surface constructions and MHD, it would be premature to conclude that indentations in our source surface correspond to shock-producing indentations in a properly computed MHD critical surface (C. F. Kennel, personal communication, 1978). The effect of indentations in an isogauss source surface for the present work is to complicate the construction of our exterior solution, probably by requiring a hydrodynamical treatment of solar-wind expansion from the source surface. Such indentations could perhaps be removed by smoothing without introducing a major error in the field configuration. We do not propose an arbitrary smoothing of the source surface as such. Rather, we contemplate diminishing the spatial resolution with which $\underset{\sim}{B}$ is described at $r = r_\odot$ (e.g., by averaging the observed $\underset{\sim}{B}$ over a larger-than-necessary area of the solar surface) so as to reduce the influence of the higher-order spherical harmonics in the vicinity of $r = r_s$. Such a procedure would tend to preserve the gross shape of the source surface while removing the bothersome indentations.

5. DISCUSSION

It appears that the general features of an MHD solution for the solar corona can be simulated quite well by use of an appropriately chosen non-spherical source surface. Moreover, the non-spherical source surface seems to generate a more satisfactory interplanetary $\underset{\sim}{B}$ field than do the more conventional spherical source surfaces of Schatten et al. (1969) and Altschuler and Newkirk (1969). We take this opportunity to discuss some of the more subtle issues that may arise in the course of implementing our model based on a non-spherical source surface.

One might ask why we have considered only the internal sources of $\underset{\sim}{B}$ in specifying the isogauss source surface, when it would have seemed more self-consistent to select an isogauss of the ultimate field configuration. We can respond to this question in several ways. First, we note that our results for the dipole case are very satisfactory, when compared with the MHD solution of Pneuman and Kopp (1971a,b). Second, we remark that the search for a self-consistent isogauss source surface would have entailed an infinite series of iterations that would have defeated our objective of defining an easily implemented procedure for calculating $\underset{\sim}{B}$. Third, we remark that the minimization of σ in (3) produces a trajectory of extremely small (ideally vanishing) total $\underset{\sim}{B}$ on the source surface, i.e., at the field cusp (see Figures 1-2) that constitutes the inner edge of the neutral sheet. Therefore, the self-consistent isogauss source surface (if definable at all) is certainly not everywhere convex, as would be required for the construction of our exterior solution.

Our source surface bears a morphological and conceptual resemblance to the self-consistent Alfvénic surface calculated in MHD by Pneuman and Kopp (1971a,b). Their Alfvénic surface (at which $\rho u^2/2 = B^2/8\pi$ for a solar wind of mass density ρ and bulk velocity $\underset{\sim}{u}$), however, was characterized by an equatorial indentation, and so was not a convex surface. Our source surface $r_s(\theta)$ is located sunward of the MHD Alfvénic surface $r_A(\theta)$ at all latitudes, i.e., is completely enclosed by the Alfvénic surface of Pneuman and Kopp (1971a,b). It is difficult to assess the importance of the inequality $r_s(\theta) < r_A(\theta)$, since, as was stated above, we do not know the fundamental mathematical relationship (if any) between source-surface constructions and MHD. The computational advantage of our source-surface approach is that we can construct coronal and interplanetary $\underset{\sim}{B}$ fields from the solar $\underset{\sim}{B}$ field without having to calculate the solar-wind properties simultaneously. However, we note that Pneuman and Kopp (1971a,b) have defined $r_A(\theta)$ without regard for the thermal energy density contained in the plasma. A differently defined $r_A(\theta)$ might have had greater significance in MHD and might also have more nearly approximated our $r_s(\theta)$.

One evident use of the results obtained above for the dipole case is the construction of a model solar wind in a prescribed $\underset{\sim}{B}$-field geometry. This has been done in exospheric theory (Lemaire and Scherer, 1971) for a prescribed radial magnetic field and in fluid theory (Durney and Pneuman, 1975) for a prescribed non-radial magnetic field, but with solar rotation neglected. It would be highly relevant to develop model solar winds in both exospheric theory and fluid theory for the present model field, which might be viewed as a prototype of reality. The present model field might also serve as a prototype for the description of cosmic-ray transport within the heliosphere. Jokipii et al. (1977) have considered the effects of gradient-curvature and other adiabatic drifts

(e.g., Northrop, 1963) on cosmic-ray transport in a model field that, unlike (31), closely resembles the present one at large distances from the sun.

We can make a qualitative comparison between interplanetary B-field observations and our results shown in Figure 6 by recognizing that our planar neutral sheet corresponds in nature to a neutral sheet that is warped about $\pm 15^{\circ}$ with respect to the heliographic equator (Schulz, 1973; Levy, 1976; Smith et al., 1978). Thus, we should interpret $\lambda \equiv |(\pi/2) - \theta|$ in Figure 6 as the angular distance of the observer from the warped neutral sheet at $r \sim 1$ AU and heliographic longitude φ, and we should interpret $\lambda = 0$ as the crossing of a "sector boundary" of the sort described by Wilcox and Ness (1965). In a superposed-epoch analysis of their observations of B, Wilcox and Ness (1965) found a relative minimum in B just past the middle of each sector (i.e., near the maximum attainable λ) and relative maxima in B just before and just after the crossing of a sector boundary. A maximum attainable λ of 15° would correspond to $\cos\theta \approx 0.26$ in Figure 6. Thus, properly interpreted, the observations of B are in good qualitative agreement with Figure 6. The maxima in B observed by Wilcox and Ness (1965) were, however, neither as pronounced nor as near the "sector boundaries" nor as symmetrical about the minimum in B as one would expect from Figure 6. Thus, the non-spherical source surface specified by (4) appears to account for the qualitative form of magnetic-field structure observed within an interplanetary sector, but the present approach must be applied to a more realistic model of the solar B field before any quantitative comparisons can be made.

Similar superposed-epoch analyses reported by Wilcox (1968) suggest nearly a doubling of the solar-wind velocity (from $u \sim 250$ km/sec to $u \sim 450$ km/sec) between the sector boundaries ($\lambda = 0$) and the middle of a sector ($\lambda \approx 15^{\circ}$ by the above interpretation). This would correspond to a latitudinal gradient $\sim$10-15 km/sec per degree of

equivalent heliomagnetic latitude and is in good agreement with the results of Rhodes and Smith (1976), who infer a gradient ~ 10-15 km/sec per degree of heliographic latitude from spacecraft observations made in and near the ecliptic plane. The present interpretation suggests that numerical uncertainties and scatter in the analysis of such spacecraft data could be reduced greatly by taking account of the observer's position within a sector, i.e., of the inferred angular distance between the observer and the warped neutral sheet.

In summary, we consider the use of a non-spherical (isogaussian) source surface to be very promising as a method of modelling the coronal and interplanetary $\underset{\sim}{B}$ field. We have demonstrated the utility of the method by constructing the prototype of a model field, i.e., that corresponding to an internal dipole surrounded by the source surface specified by (4). We anticipate the application of our method to more realistic representations of the solar $\underset{\sim}{B}$ field, but we recognize that considerable work remains to be done before this goal is fully achieved.

REFERENCES

Altschuler, M. D., and Newkirk, G., Jr.: 1969, Solar Phys., 9, 131.

Altschuler, M. D., Levine, R. H., Stix, M., and Harvey, J. W.: 1977, Solar Phys., 51, 345.

Dessler, A. J.: 1967, Rev. Geophys., 5, 1.

Durney, B., and Pneuman, G. W.: 1975, Solar Phys., 40, 461.

Durney, B. R., and Roberts, P. H.: 1971, Astrophys. J., 170, 319.

Hundhausen, A. J.: 1970, Rev. Geophys. Space Phys., 8, 729.

Hundhausen, A. J.: 1977, in J. B. Zirker (ed.), Coronal Holes and High Speed Wind Streams, Colorado Assoc. Univ. Press, Boulder, p. 225.

Jokipii, J. R., Levy, E. H., and Hubbard, W. B.: 1977, Astrophys. J., 213, 861.

Kennel, C. F.: 1978, personal communication.

Lemaire, J., and Scherer, M.: 1971, J. Geophys. Res., 76, 7479.

Levine, R. H.: 1977, personal communication.

Levy, E. H.,: 1976, Nature, 261, 394.

Northrop, T. G.: 1963, The Adiabatic Motion of Charged Particles, Wiley-Interscience, New York, pp. 6-8.

Parker, E. N.: 1958, Astrophys. J., 128, 664.

Pneuman, G. W., and Kopp, R. A.: 1971a, Solar Phys., 18, 258.

Pneuman, G. W., and Kopp, R. A.: 1971b, in R. A. Howard (ed.), Solar Magnetic Fields, I.A.U. Symp. 43, Reidel, Dordrecht, pp. 526-533.

Rhodes, E. J., Jr., and Smith, E. J.: 1976, J. Geophys. Res., 81, 2123.

Schatten, K. H.: 1971, Cosmic Electrodyn., 2, 232.

Schatten, K. H., Wilcox, J. M., and Ness, N. F.: 1969, Solar Phys., 6, 442.

Schulz, M.: 1973, Astrophys. Space Sci., 24, 371.

Smith, E. J., Tsurutani, B. T., and Rosenberg, R. L.: 1978, J. Geophys. Res., 83, 717.

Thomas, G. B., Jr.: 1960, Calculus and Analytic Geometry, Addison-Wesley, Reading, Mass., p. 589.

Wilcox, J. M.: 1968, Space Sci. Rev., 8, 258.

Wilcox, J. M., and Ness, N. F.: 1965, J. Geophys. Res., 70, 5793.

Yeh, T., and Pneuman, G. W.: 1977, Solar Phys., 54, 419.

Zirker, J. B. (ed.): 1977, Coronal Holes and High Speed Wind Streams, Colorado Assoc. Univ. Press, Boulder.

THE IVAN A. GETTING LABORATORIES

The Laboratory Operations of The Aerospace Corporation is conducting experimental and theoretical investigations necessary for the evaluation and application of scientific advances to new military concepts and systems. Versatility and flexibility have been developed to a high degree by the laboratory personnel in dealing with the many problems encountered in the nation's rapidly developing space and missile systems. Expertise in the latest scientific developments is vital to the accomplishment of tasks related to these problems. The laboratories that contribute to this research are:

Aerophysics Laboratory: Launch and reentry aerodynamics, heat transfer, reentry physics, chemical kinetics, structural mechanics, flight dynamics, atmospheric pollution, and high-power gas lasers.

Chemistry and Physics Laboratory: Atmospheric reactions and atmospheric optics, chemical reactions in polluted atmospheres, chemical reactions of excited species in rocket plumes, chemical thermodynamics, plasma and laser-induced reactions, laser chemistry, propulsion chemistry, space vacuum and radiation effects on materials, lubrication and surface phenomena, photosensitive materials and sensors, high precision laser ranging, and the application of physics and chemistry to problems of law enforcement and biomedicine.

Electronics Research Laboratory: Electromagnetic theory, devices, and propagation phenomena, including plasma electromagnetics; quantum electronics, lasers, and electro-optics; communication sciences, applied electronics, semiconducting, superconducting, and crystal device physics, optical and acoustical imaging; atmospheric pollution; millimeter wave and far-infrared technology.

Materials Sciences Laboratory: Development of new materials; metal matrix composites and new forms of carbon; test and evaluation of graphite and ceramics in reentry; spacecraft materials and electronic components in nuclear weapons environment; application of fracture mechanics to stress corrosion and fatigue-induced fractures in structural metals.

Space Sciences Laboratory: Atmospheric and ionospheric physics, radiation from the atmosphere, density and composition of the atmosphere, aurorae and airglow; magnetospheric physics, cosmic rays, generation and propagation of plasma waves in the magnetosphere; solar physics, studies of solar magnetic fields; space astronomy, x-ray astronomy; the effects of nuclear explosions, magnetic storms, and solar activity on the earth's atmosphere, ionosphere, and magnetosphere; the effects of optical, electromagnetic, and particulate radiations in space on space systems.

THE AEROSPACE CORPORATION
El Segundo, California

• • •

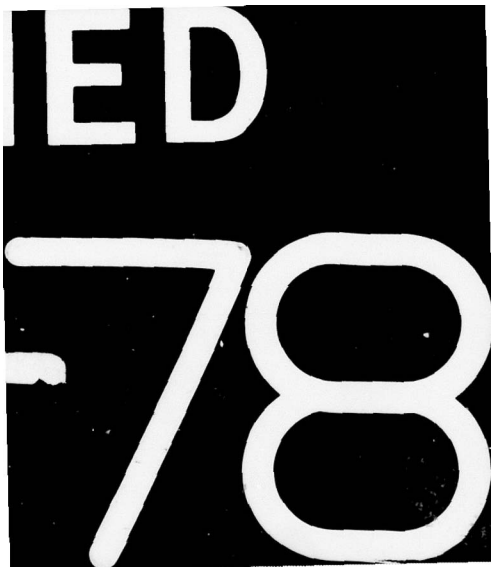
ED
78